Electronically Supplementary Information for

Novel nitrogen-rich conjugated microporous polymers for efficient capture of iodine and methyl iodide

Jiaxin Yang, [a] Shenglin Wang, [a] Qianqian Yan, [a] Hui Hu,*[,a] Huanjun Xu,[b] Haibin Ma,[c,*] Xiaofang Su,[a] and Yanan Gao*[,a]

a. Key Laboratory of Ministry of Education for Advanced Materials in Tropical Island Resources, Hainan University, No 58, Renmin Avenue, Haikou 570228, China

b. School of Science, Qiongtai Normal University, Haikou 571127, China

c. College of Chemistry, Chemical & Environmental Engineering, Weifang 261061, China

E-mail: hhu@hainanu.edu.cn; haibinwfc@126.com; ygao@hainanu.edu.cn

Characterization

Solution ^{1}H and ^{13}C NMR spectra were recorded on a Bruker 400 MHz NMR spectrophotometer. Solid-state ^{13}C CM/MAS NMR spectra were measured on a Bruker AVANCE III 600 MHz spectrometer. The electronic absorption spectra were recorded on a JASCO model V-770 spectrophotometer. Fourier-transform infrared (FT-IR) spectra were detected on a Jasco model FT/IR-6800 infrared spectrophotometer with a scan number of 32, and the background was subtracted. Powder X-ray diffraction (PXRD) data were performed on a Rigaku Smart Lab X-ray diffractometer with Cu K_{α} radiation (λ = 1.540598 Å) by depositing powder on glass substrate to measure at 2θ from 2 to 30º with a 0.05º increment. N_2 and CO_2 adsorption analyses were performed by using QUANTACHROME AUTOSORB-IQ2 to analyze the specific surface area, pore size distributions. Before measurement, powder samples were degassed under a dynamic vacuum at 120 ℃ for 15 h. Brunauer Emmett-Teller (BET) surface areas were calculated from the linear region of the N_2 isotherm at 77 K within the pressure range P/P_0 of 0.003–0.05 using micropore BET assistant on the ASiQwin software. Pore size distributions were determined using the quenched solid density functional theory (QSDFT) method. Thermogravimetric analysis (TGA) was recorded on a mettler TG-DSC 3+ under N_2 at a heating rate of 10 ℃ min^{-1} from ambient temperature to 800 °C. Elemental analysis (EA) of C, H and N was collected by Vario EL cube (Elementar, Germany) elemental analyzer. Field emission scanning electron microscopy (FE SEM) was

measured on the scanning electron microscopy (Gemini300, ZEISS Germany) at 3.0 kV acceleration voltage. High-resolution transmission electron microscope (HR-TEM) analysis was recorded on FEI Tecnai G2 F30 electron microscope. The Raman spectra were obtained using an inVia Qontor Evolution Raman spectrometer with a 532 nm laser. The X-ray photoelectron spectroscopy (XPS) was carried out by a Thermo Scientiffc Escalab 250Xi.

Synthetic route and characterization of Car-4CHO

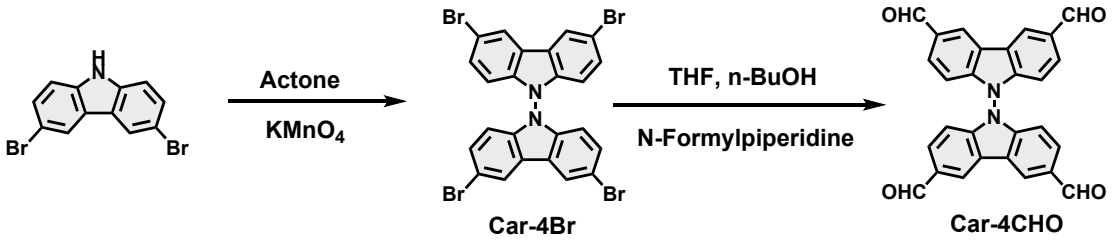

Scheme S1. The procedure for the synthesis of Car-4CHO.

3,3',6,6'-Tetraformyl-9,9'-bicarbazole (Car-4CHO) was synthesized according to a modified method reported in the literature.[1] To a 100 mL two-neck bottle was added 3,6-dibromocarbazole (1.625 g), $KMnO_4$ (1.975 g), and acetone (30 mL) under a nitrogen atmosphere. The mixture was then refluxed at 70 °C for 10 hours. Once the reaction was finished, ultrapure water was added and a lemon-yellow solid was obtained. The crude product was collected through suction filtration. Car-4Br was obtained as a white powder solid after recrystallization from methanol in 79% yield.

Under a nitrogen atmosphere, Car-4Br (1.3 g) and ultra-dry tetrahydrofuran (60 mL) were weighted into a 500 mL three-neck reaction flask. The reaction was stirred for 10 minutes. The resulting mixture was then transferred to a low-temperature reactor set at -78 °C. Once the temperature stabilized, 1.6 M n-butyllithium (13.5 mL) was dropwise added within 30 minutes, and the reaction was stirred at -78 °C for 3

hours. Upon completion of the reaction, 2.5 mL piperidine-1-carboxaldehyde was dropwise added within 20 minutes, and the reaction was left to proceed overnight at room temperature. After that, 100 mL of 6 M hydrochloric acid was added, and the mixture was stirred for 30 minutes to ensure complete hydrolysis. The resulting mixture was extracted five times with ethyl acetate/water, and then dried to obtain a crude product. Recrystallization with acetone yielded a white Car-4CHO powder in a 25% yield. The NMR spectra were shown in Figure S1-S3.

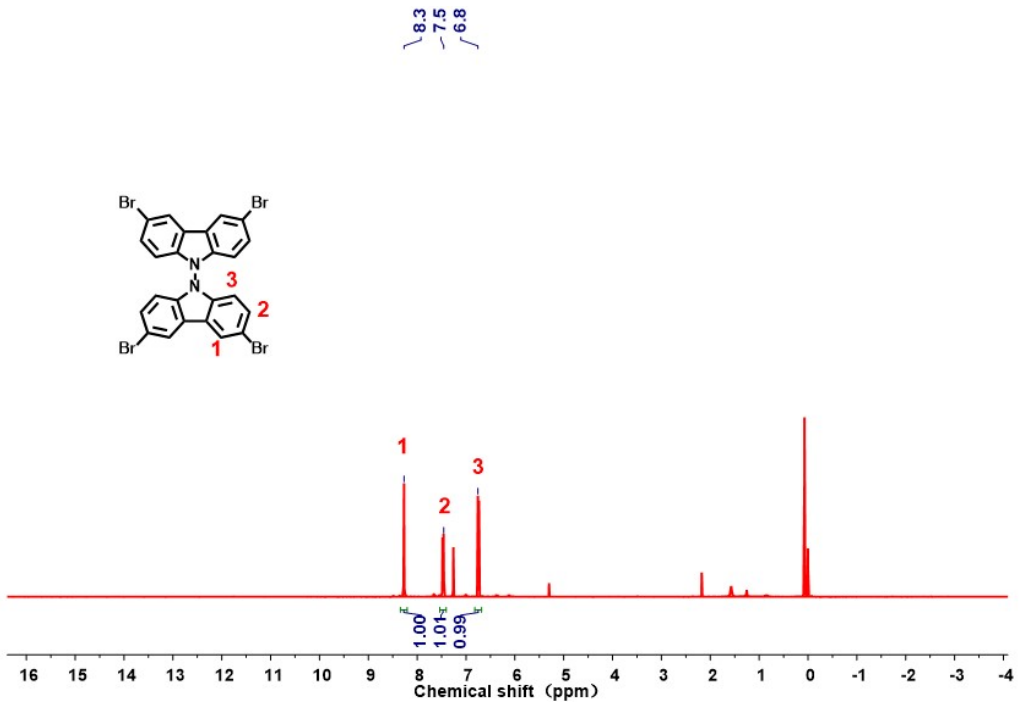

Fig. S1. ^{1}H NMR spectra of Car-4Br.

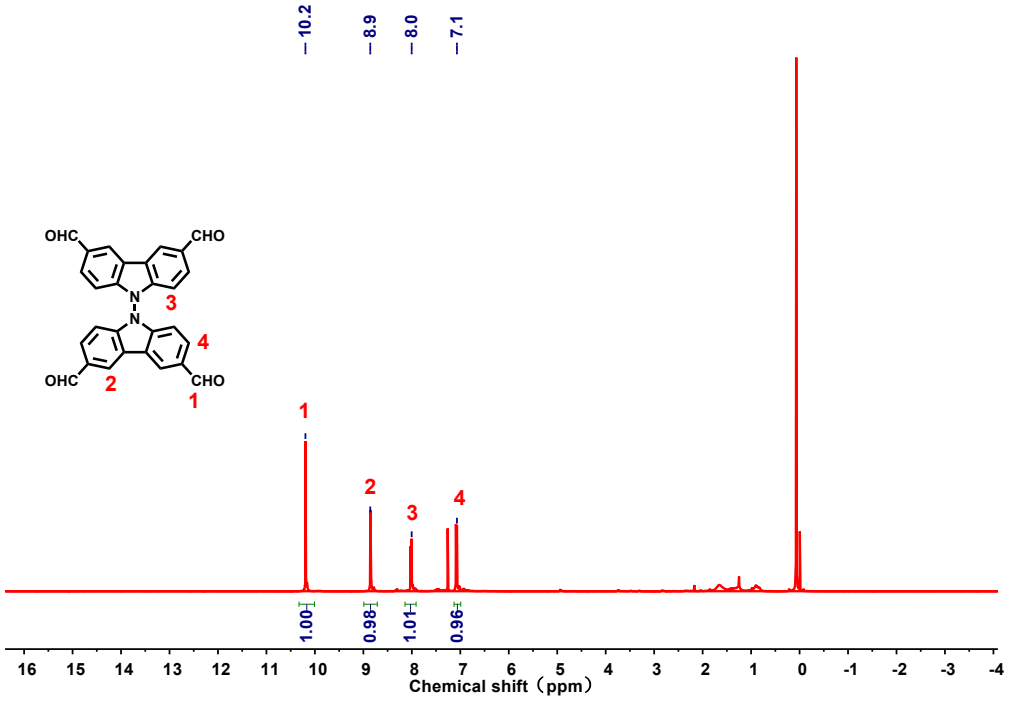

Fig. S2. ^{1}H NMR spectra of Car-4CHO.

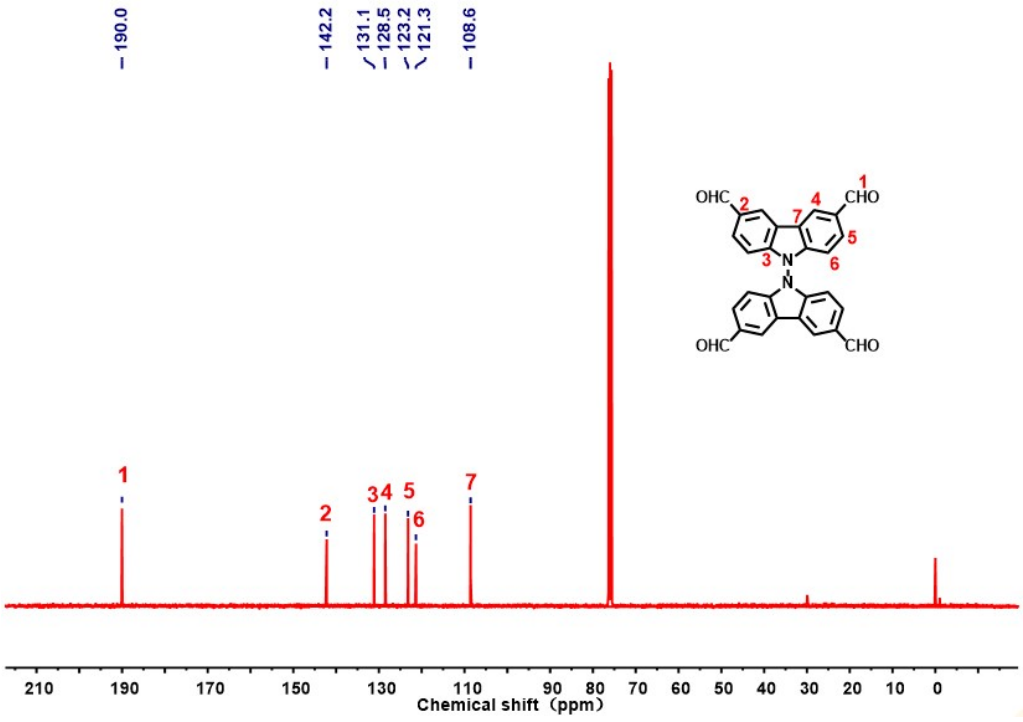

Fig. S3. ^{13}C NMR spectrum of Car-4CHO.

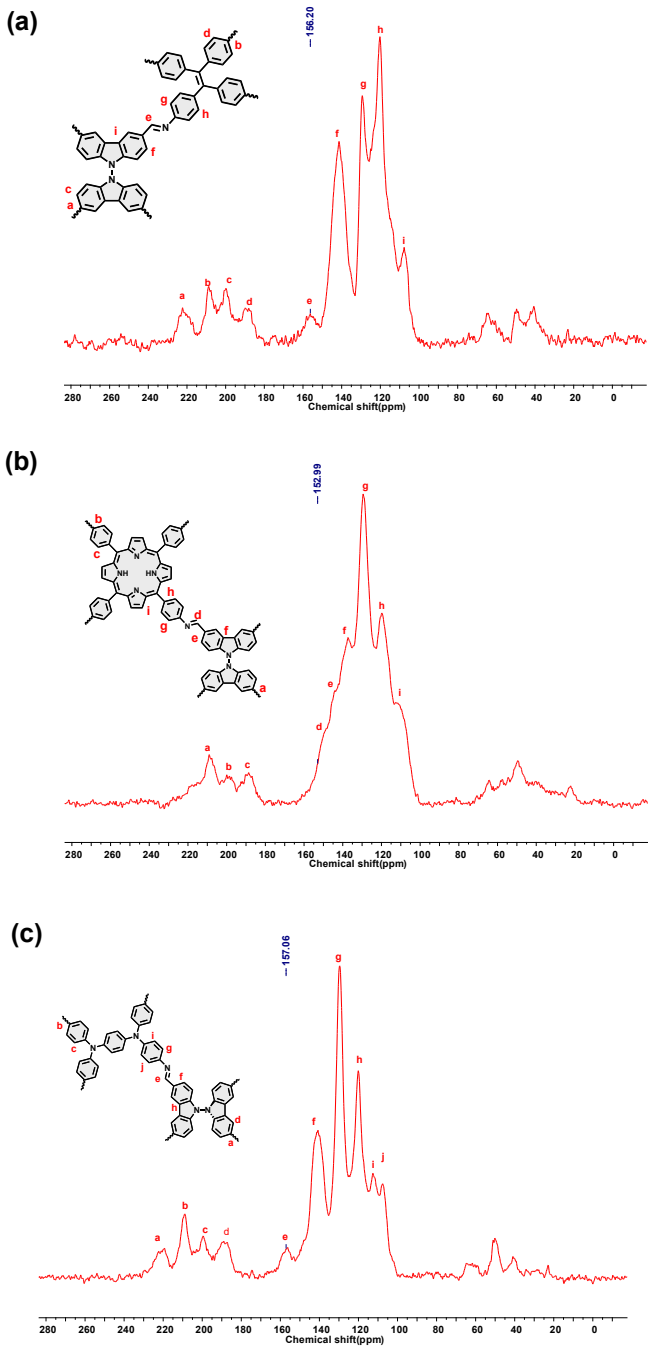

Fig. S4 Solid state ^{13}C CP/MAS NMR of Car-CMPs.

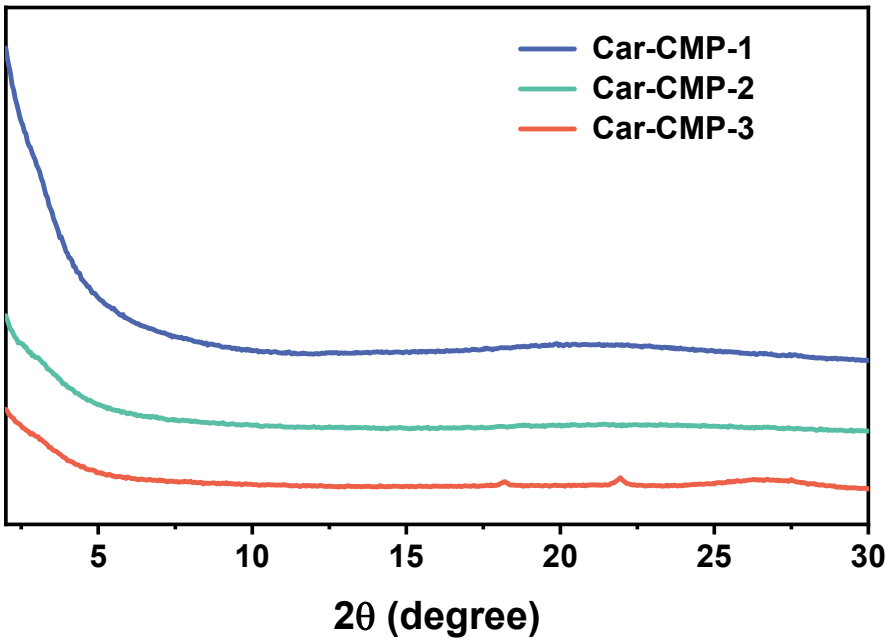

Fig. S5 Powder X-ray diffraction (PXRD) profiles of Car-CMPs.

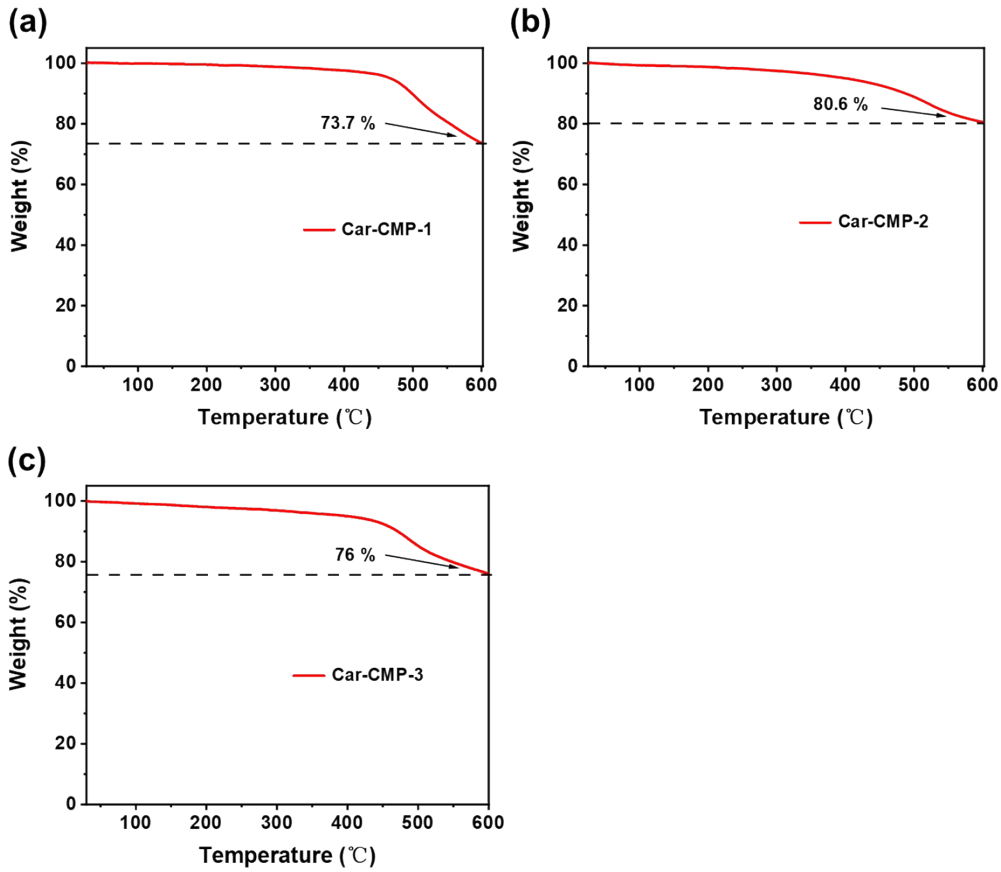

Fig. S6 TGA curves of Car-CMP-1 (a), Car-CMP-2 (b) and Car-CMP-3 (c).

Table. S1 Elemental analysis of Car-CMPs.

Samples		C%	H%	N%
Car-CMP-1	Found	81.67	3.91	9.38
	Caled.	84.48	4.22	10.99
Car-CMP-2	Found	78.01	3.34	10.92
	Caled.	82.58	4.04	13.38
Car-CMP-3	Found	78.09	4.443	13.09
	Caled.	82.44	4.29	13.26

Iodine vapor adsorption experimental procedure. A certain amount of CMP sample and excess I_2 solid were separately loaded into two small vials and then transferred

them into a big chamber. The chamber was sealed tightly and moved to a convection oven (348 K) for iodine vapor adsorption experiment under ambient pressure. The weight of the vial that loaded CMPs was recorded at different exposure times and the adsorption curves of the samples were thus plotted.

The iodine uptake capacity of CMPs was evaluated according to the following equation:

$$\alpha = \frac{(m_2 - m_1)}{m_1}$$

where α is the iodine vapor uptake capacity, and m_1 and m_2 represent the weight of CMP sample before and after the iodine capture.

Reusability of the CMPs. Initially, the iodine saturated-adsorbed CMP sample (0.1 mg) was dispersed with methanol (3.0 mL) with vigorous stirring for a specified duration. The resulting mixture was then separated, and the collected supernatant was filtered using a 0.22 μm Millipore cellulose membrane before UV-vis absorption analysis. To assess reusability, the iodine saturated-adsorbed CMP sample underwent Soxhlet-extraction to completely remove iodine from I_2@BC-CMP-1, I_2@BC-CMP-2, and I_2@BC-CMP-3 with methanol. Subsequently, the empty samples were dried at 80 °C for 48 hours and reused for iodine vapor absorption in another adsorption cycle. This entire process was repeated for a total of five cycles.

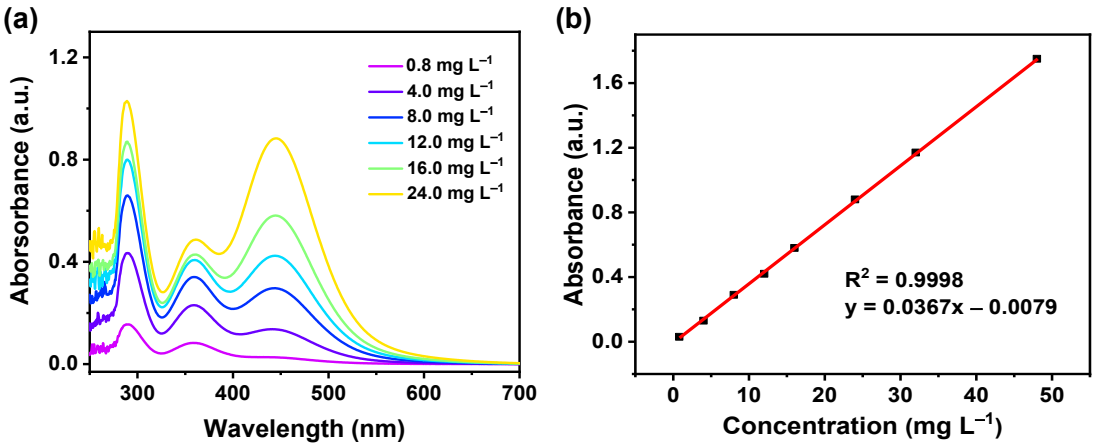

Fig. S7 UV-vis spectral of methanol standard solutions of iodine with different concentrations (a) and the corresponding calibration curve of absorbance versus iodine concentration (b) established from UV-vis spectra as shown in (a).

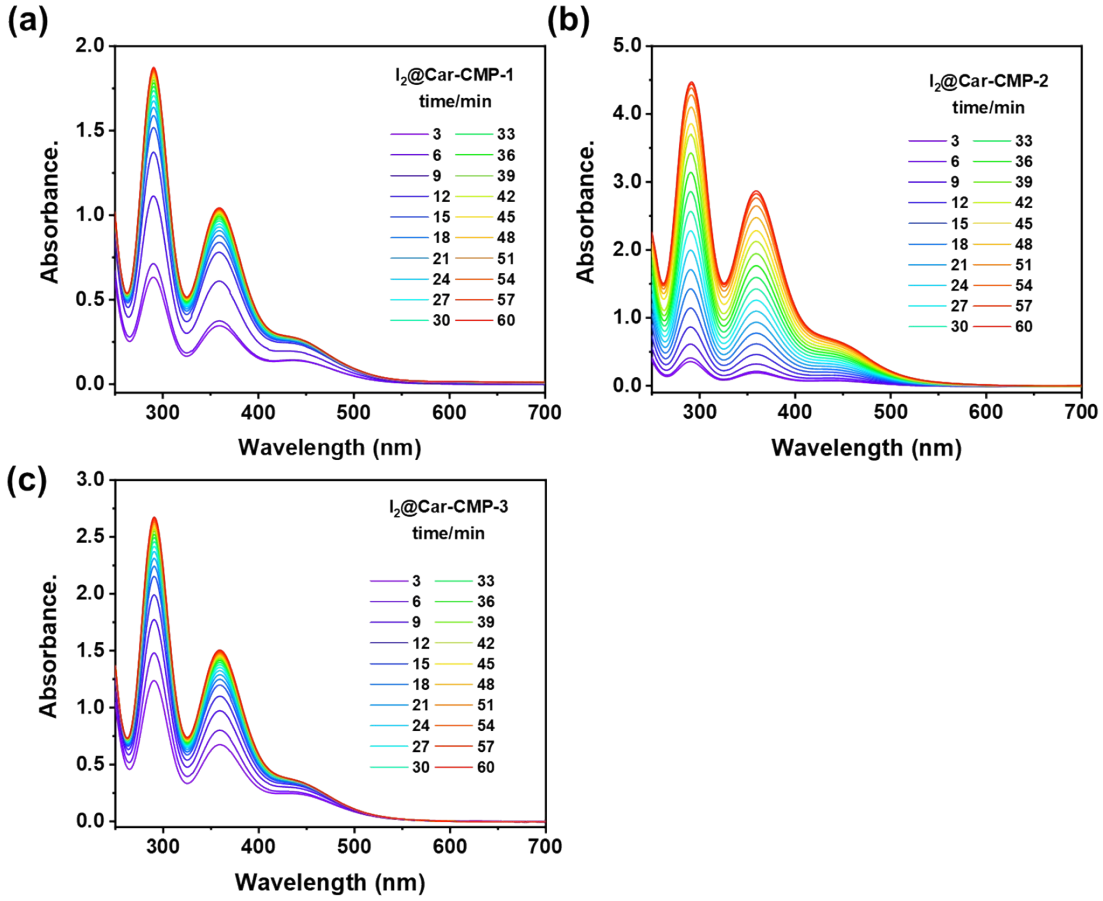

Fig. S8 Temporal evolution of UV-vis adsorption spectral for the delivery of iodine from I_2@Car-CMP-1 (a), I_2@Car-CMP-2 (b), and I_2@Car-CMP-3 (c).

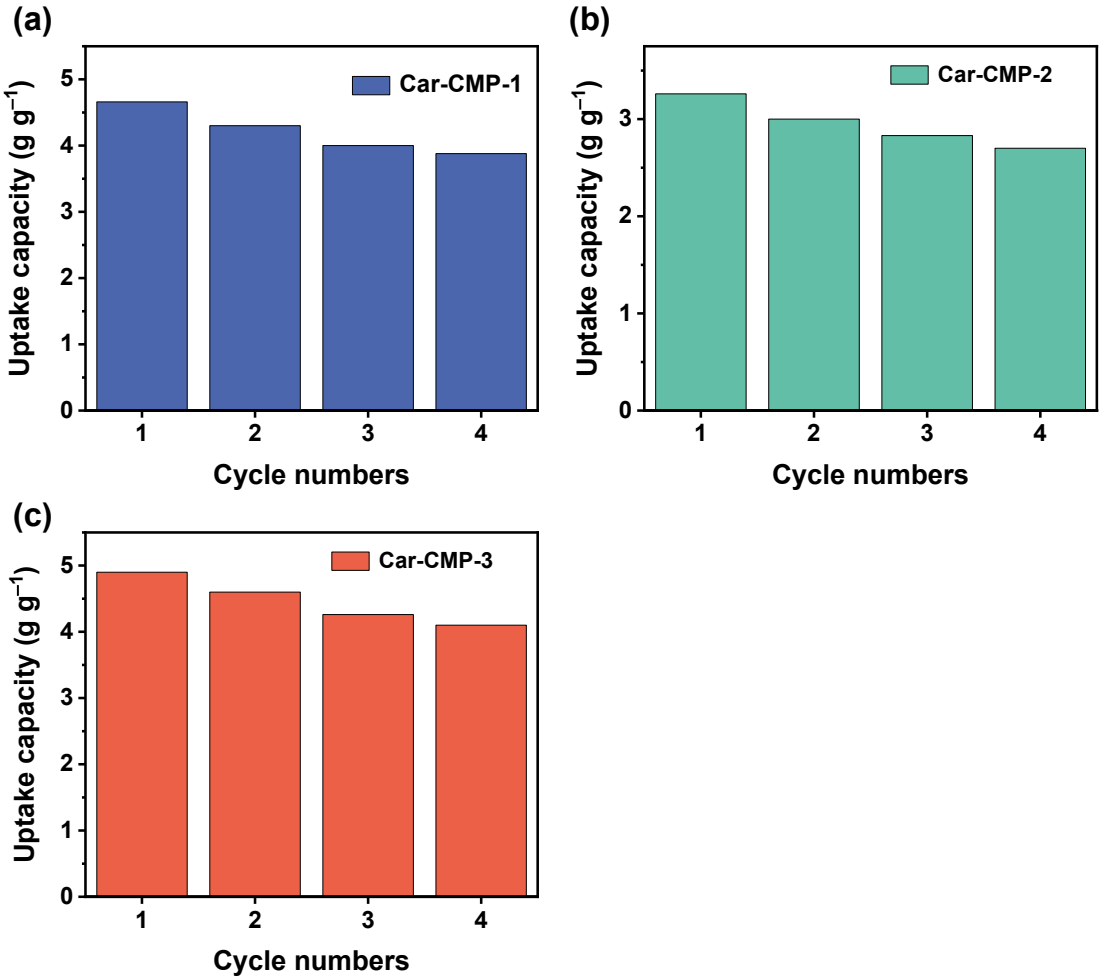

Fig. S9 Recyclability of Car-CMP-1 (a), Car-CMP-2 (b) and Car-CMP-3 (c).

Experiment procedures of iodine adsorption in n-hexane. The I_2 adsorption experiment of CMPs was also carried out in n-hexane solution of iodine. A series of iodine-n-hexane solutions (10.0 mL) with different concentrations (200 mg·L^{-1}, 400 mg·L^{-1}, 600 mg·L^{-1}, 800 mg·L^{-1} and 1000 mg·L^{-1}, respectively) were first prepared.

Then, Car-CMPs (3.0 mg) was dispersed in the solution (5 mL) for a given time at room temperature. The mixture was isolated and the supernatant was filtered with 0.22 μm Millipore cellulose membrane before UV-visible absorption spectrum analysis. The saturated adsorption amount of iodine in the n-hexane solutions was measured after 72 hours' adsorption. The iodine uptake capacity of CMPs in solution was evaluated according to the following equation:

$$R = \frac{(C_0 - C_t)}{C_0} \qquad Q_t = \frac{(C_0 - C_t)}{W} * V$$

where R is the iodine removal rate of CMPs in n-hexane solution and Q_t is the adsorption value of iodine in the solution at a given time. C_t represents the iodine concentration of the supernatant after adsorption of iodine, C_0 represents the iodine concentration of the initial supernatant, V represents the volume of n-hexane solution, and W represents the mass of CMPs.

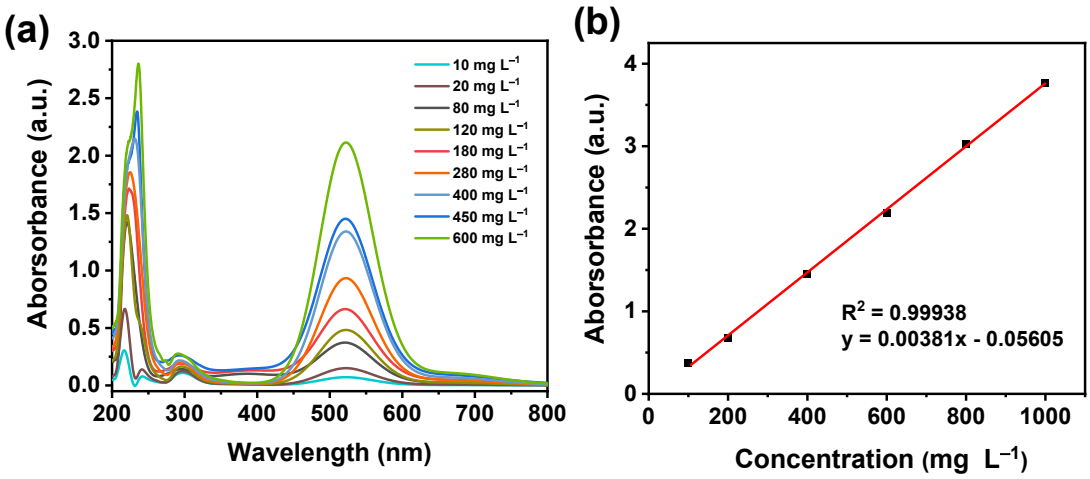

Fig. S10 UV-vis spectral of n-hexane standard solutions of iodine with different concentrations (a) and the corresponding calibration curve of absorbance versus iodine concentration (b) established from UV-vis spectra as shown in (a).

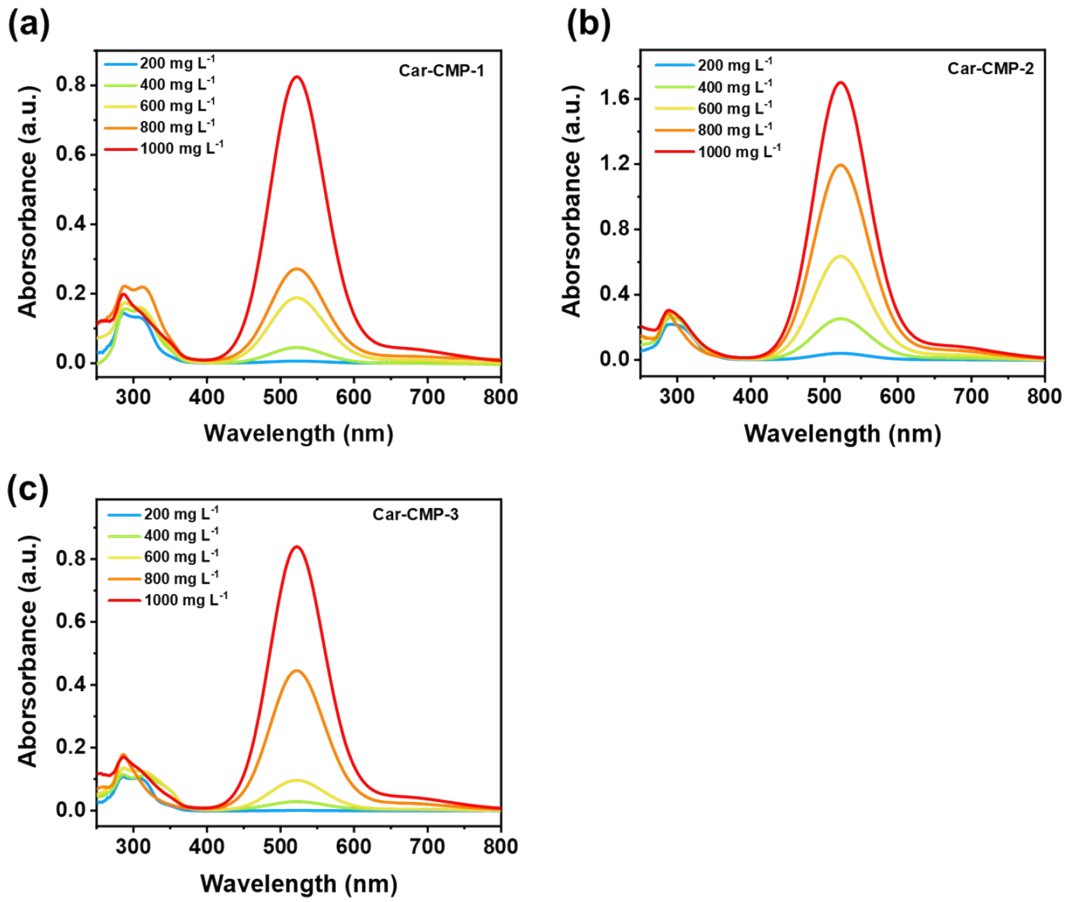

Fig. S11 UV-vis absorption spectra of iodine in n-hexane solution (200 mg L^{-1}, 400 mg L^{-1}, 600 mg L^{-1}, 800 mg L^{-1} and 1000 mg L^{-1}) after the uptake by Car-CMP-1 (a), Car-CMP-2 (b) and Car-CMP-3 (c) for 72 h.

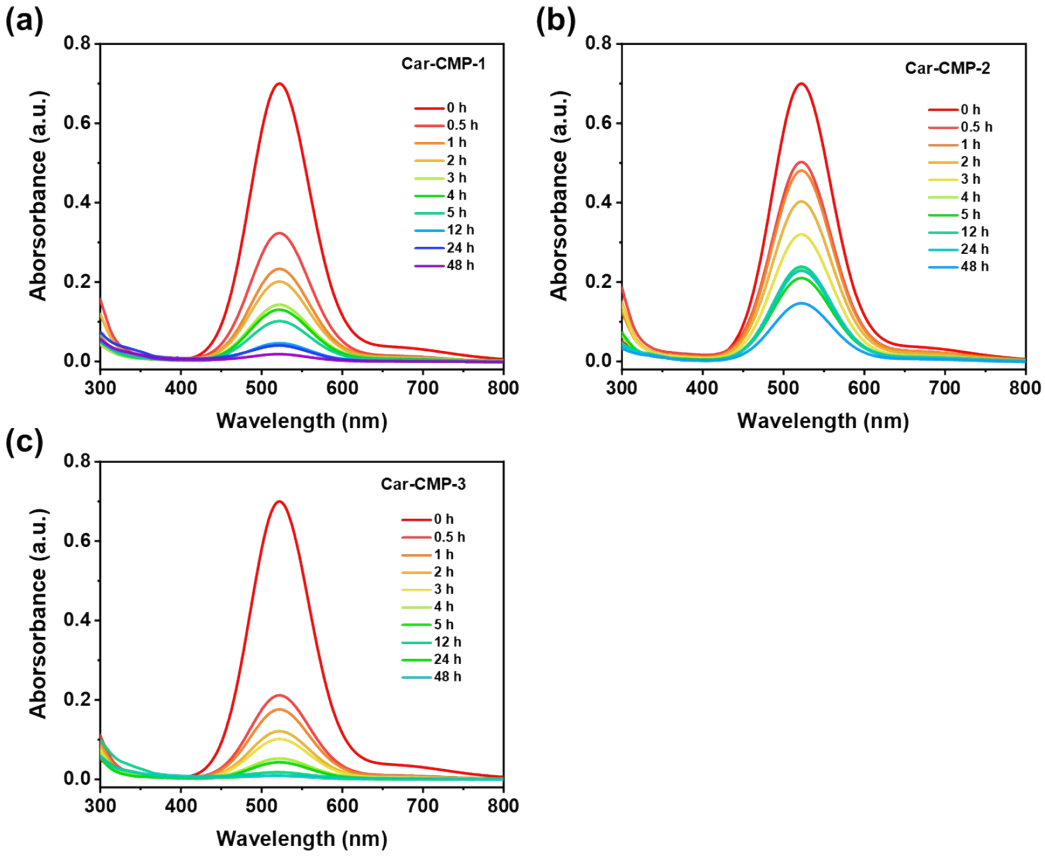

Fig. S12 Temporal evolution of UV-vis adsorption spectral for the iodine capture by Car-CMP-1 (a), Car-CMP-2 (b) and Car-CMP-3 (c).

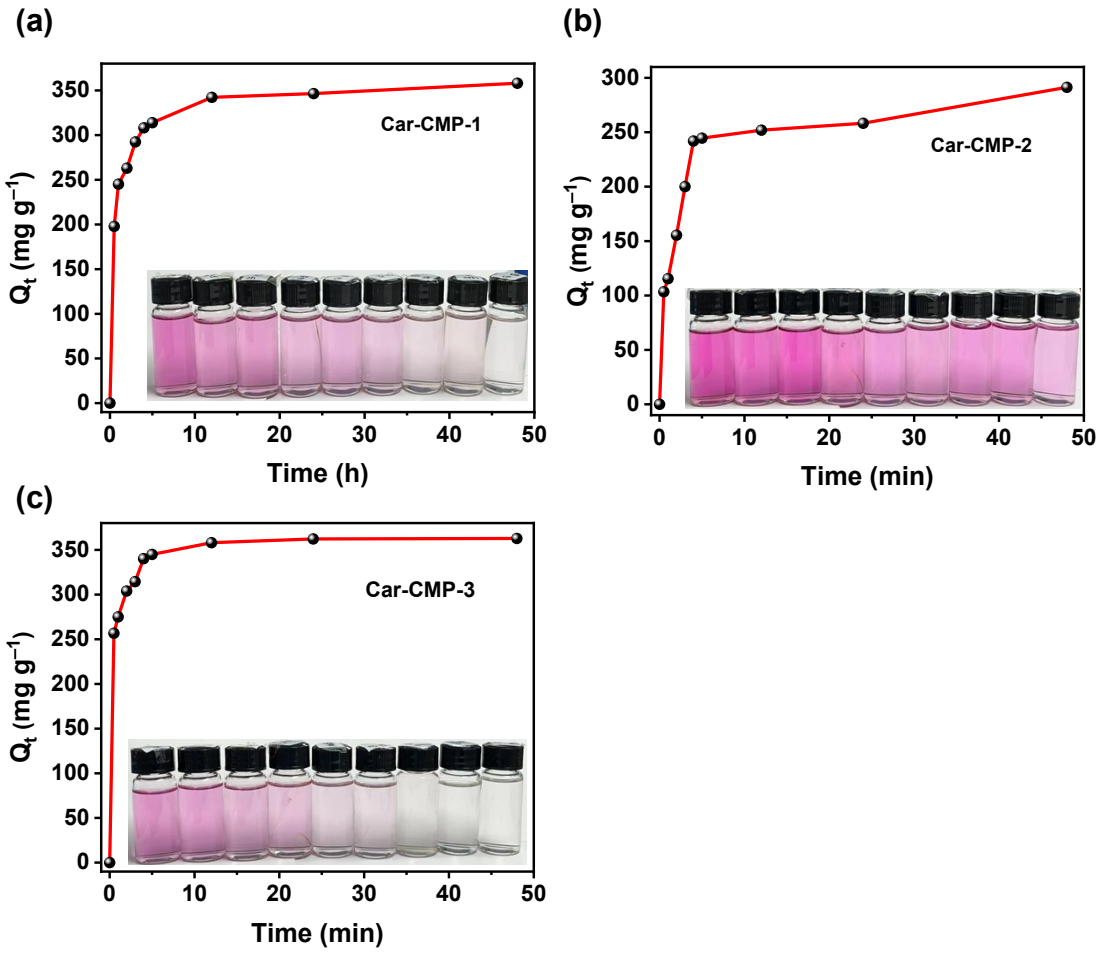

Fig. S13 Temporal evolution of the iodine capture by Car-CMP-1 (a), Car-CMP-2 (b) and Car-CMP-3 (c).

Table. S2 The parameters of two kinds of kinetic models

Models	Pseudo-first-order model			Pseudo-second-order model		
Parameters	q_e	K_1	R^2	q_e	K_2	R^2
Car-CMP-1	358.0086	0.0971	0.9470	358.0086	0.0042	0.9999
Car-CMP-2	291.3419	0.0961	0.9037	291.3419	0.0023	0.9971
Car-CMP-3	362.7330	0.1054	0.7268	362.7330	0.0087	0.9999

The Pseudo-first-order model: $\ln(q_e - q_t) = \ln q_e - K_1 t$ （S1）

The Pseudo-second-order model： $\frac{t}{q_t} = \frac{1}{K_2 q_e^2} + \frac{t}{q_e}$ （S2）

Where, q_t (mg g^{-1}): The amount of iodine adsorbed at time t；

q_e (mg g^{-1}): The amount of iodine adsorbed at adsorption equilibrium；

k_1 (h^{-1}): The seudo first-order rate constant ；

k_2 (g mg^{-1} h^{-1}): The seudo second-order rate constant；

R^2: The coefficient of determination.

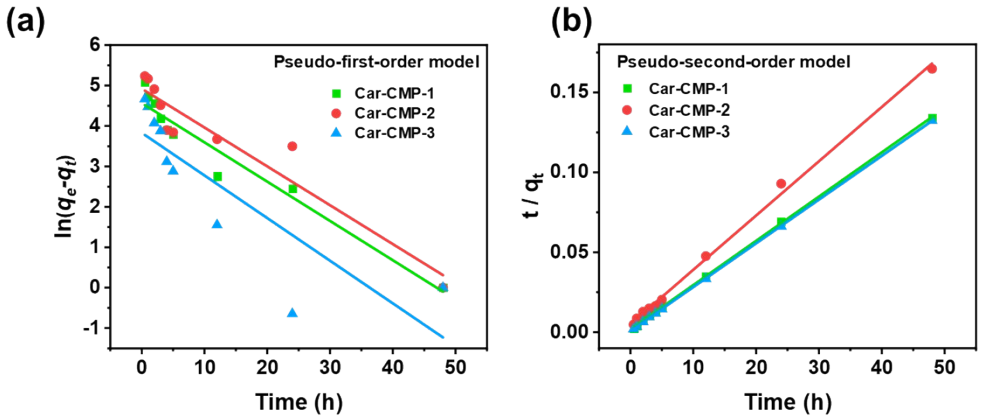

Fig. S14 Pseudo-first-order (a) and Pseudo-second-order (b) linear fitting plots for iodine capture in n-hexane solutions by Car-CMPs.

Table S3. Comparison of representatively reported adsorbents with our work for iodine vapor adsorption under atmospheric pressure.

Sample	BET ($m^2\ g^{-1}$)	Capture of iodine vapor ($g\ g^{-1}$)	Ads. temp	Ads. time	Ref.
COF-TAPT	2348	8.61	75 °C	96 h	2
COF-TAPB	2290	7.94	75 °C	96 h	2
TFB-DB COF	-	6.40	75 °C	72 h	3
TFB-BD COF	-	6.23	75 °C	72 h	3
QTD-COF-V	-	6.29	75 °C	4 h	3
TPB-DMTP COF	1927	6.26	75 °C	96 h	4
TJNU-203	1833	5.88	77 °C	120 h	5
TJNU-201	2510	5.62	75 °C	96 h	6
TPT-BD COF	109	5.43	75 °C	46 h	3
TTDP-1	12	5.3	75 °C	22 h	7
CMP-LS8	2028	5.29	75 °C	12 h	**8**
QTD-COF-3	-	5.16	75 °C	6 h	3
Car-CMP-3	450	5.10	75 °C	120 h	**This work**
CMPN	86.2	5.02	60 °C	140 h	**9**
Car-CMP-1	305	4.98	75 °C	120 h	**This work**
TTA-TTB COF	1733	4.95	75 °C	96 h	4
DbTd-COF	368	4.93	75 °C	48 h	10
CSUCPOP-1	1032	4.9	75 °C	30 h	11
QTD-COF-4	-	4.85	75 °C	4 h	3
TJNU-202	714	4.82	75 °C	96 h	6
ETTA-TPA	1822	4.79	75 °C	96 h	4
TTDP-2	7	4.7	75 °C	22 h	7
TPE-PyTTA-CMP	-	4.68	75 °C	120 h	12
QTD-COF-1	-	4.67	75 °C	4 h	3
TPT-DHBD25 COF	188	4.65	75 °C	46 h	3

DaTd-COF	275	4.48	75 ℃	48 h	10
CMP-LS5	-	4.4	75 ℃	110 h	13
TPT-DHBD50 COF	124	4.30	75 ℃	46 h	3
TTDP-3	13	4.2	75 ℃	22 h	7
i-POP-BPTM-3	1485	4.15	77 ℃	24 h	14
TPT-DHBD75 COF	157	4.12	75 ℃	46 h	3
CSUCPOP-2	555	4.1	75 ℃	30 h	11
P-DPDA	24	4.08	75 ℃	8 h	15
TPT-DHBD COF	297	4.03	75 ℃	46 h	3
i-POP-BPTM-2	1611	3.75	77 ℃	24 h	14
TPE-TAPP-CMP	-	3.67	75 ℃	120 h	12
DpTd-COF	127	3.43	75 ℃	48 h	10
i-POP-BPTM-1	1753	3.42	77 ℃	24 h	14
Car-CMP-2	412	3.38	75 ℃	120 h	**This work**
P-TPB	646	3.35	75 ℃	8 h	15
CMP-LS4	-	3.32	75 ℃	110 h	13
CSUCPOP-3	269	3.3	75 ℃	30 h	11
Bpy-Cage	1.8	3.23	75 ℃	24 h	16
BTPOC	52	3.21	75 ℃	50 h	17
HCMP3	82	3.16	75 ℃	110 h	18
PTPATTh	-	3.13	75 ℃	60 h	19
TPE-TPDA-CMP	-	3.1	75 ℃	120 h	12
QTD-COF-2	-	2.87	75 ℃	5 h	3
COF-TpgDB	209	2.75	125 ℃	72 h	20
PTPATCz	-	2.56	75 ℃	60	19
CMP-LS6	-	2.44	75 ℃	110 h	13
ImCMP-1	-	2.36	80 ℃	8 h	21
COF-TpgBD	217	1.81	125 ℃	72 h	20
COF-TpgTd	303	1.66	125 ℃	72 h	20

CMPs are marked in bold

Table S4. Comparison of representatively reported adsorbents with our work for CH_3I adsorption under atmospheric pressure.

Sample	BET ($m^2\ g^{-1}$)	Capture of CH_3I vapor ($g\ g^{-1}$)	Ads. temp (°C)	Ads. time (h)	Ref.
Car-CMP-3	450	1.90	75	120	**This work**
SCU-20	34.8	1.84	75	120	[22]
Car-CMP-1	305	1.61	75	120	**This work**
TTA-DMTP-COF	2332	1.6	75	70	[23]
COF-TAPT	2348	1.53	25	100	[2]
SCU-COF-2	-	1.45	25	120	[24]
TFPA-TAPT	-	1.37	25	100	[2]
Car-CMP-2	412	1.10	75	120	**This work**
COF-TAPB	2290	0.81	25	100	[2]
COF-A	1560	0.43	25	70	[25]
COF-C	1185	0.36	25	70	[25]
COF-D	1013	0.35	25	70	[25]

Reference

1. S. Feng, H. Xu, C. Zhang, Y. Chen, J. Zeng, D. Jiang and J.-X. Jiang, *Chemical Communications*, 2017, **53**, 11334-11337.
2. Y. Xie, T. Pan, Q. Lei, C. Chen, X. Dong, Y. Yuan, W. A. Maksoud, L. Zhao, L. Cavallo, I. Pinnau and Y. Han, *Nature Communications*, 2022, **13**, 2878.
3. X. Guo, Y. Li, M. Zhang, K. Cao, Y. Tian, Y. Qi, S. Li, K. Li, X. Yu and L. Ma, *Angewandte Chemie International Edition*, 2020, **59**, 22697-22705.
4. P. Wang, Q. Xu, Z. Li, W. Jiang, Q. Jiang and D. Jiang, *Advanced Materials*, 2018, **30**, 1801991.
5. L. Zhang, J. Li, H. Zhang, Y. Liu, Y. Cui, F. Jin, K. Wang, G. Liu, Y. Zhao and Y. Zeng, *Chemical Communications*, 2021, **57**, 5558-5561.
6. X. Guo, Y. Tian, M. Zhang, Y. Li, R. Wen, X. Li, X. Li, Y. Xue, L. Ma, C. Xia and S. Li, *Chemistry of Materials*, 2018, **30**, 2299-2308.
7. W. Du, Y. Qin, C. Ni, W. Dai and J. Zou, *ACS Applied Polymer Materials*, 2020, **2**, 5121-5128.
8. S. Wang, Q. Hu, Y. Liu, X. Meng, Y. Ye, X. Liu, X. Song and Z. Liang, *Journal of Hazardous Materials*, 2020, **387**, 121949.
9. M. Xu, T. Wang, L. Zhou and D. Hua, *Journal of Materials Chemistry A*, 2020, **8**, 1966-1974.
10. Z. Wu, W. Wei, J. Ma, J. Luo, Y. Zhou, Z. Zhou and S. Liu, *ChemistrySelect*, 2021, **6**, 10141-10148.
11. S. Xiong, X. Tang, C. Pan, L. Li, J. Tang and G. Yu, *ACS Applied Materials & Interfaces*, 2019, **11**, 27335-27342.
12. S. Luo, Q. Yan, S. Wang, H. Hu, S. Xiao, X. Su, H. Xu and Y. Gao, *ACS Applied Materials & Interfaces*, 2023, **15**, 46408-46416.
13. S. Wang, Y. Liu, Y. Ye, X. Meng, J. Du, X. Song and Z. Liang, *Polymer Chemistry*, 2019, **10**, 2608-2615.
14. Z. Li, H. Li, D. Wang, A. Suwansoontorn, G. Du, Z. Liu, M. M. Hasan and Y. Nagao, *Polymer*, 2020, **204**, 122796.
15. J. Wang, C. Wang, H. Wang, B. Jin, P. Zhang, L. Li and S. Miao, *Microporous and Mesoporous Materials*, 2021, **310**, 110596.
16. D. Luo, Y. He, J. Tian, J. L. Sessler and X. Chi, *Journal of the American Chemical Society*, 2022, **144**, 113-117.
17. C. Liu, Y. Jin, Z. Yu, L. Gong, H. Wang, B. Yu, W. Zhang and J. Jiang, *Journal of the American Chemical Society*, 2022, **144**, 12390-12399.
18. Y. Liao, J. Weber, B. M. Mills, Z. Ren and C. F. J. Faul, *Macromolecules*, 2016, **49**, 6322-6333.
19. T. Geng, G. Chen, H. Xia, W. Zhang, Z. Zhu and B. Cheng, *Journal of Solid State Chemistry*, 2018, **265**, 85-91.
20. Y. Sun, S. Song, D. Xiao, L. Gan and Y. Wang, *ACS Omega*, 2020, **5**, 24262-24271.

21. X. Meng, Y. Liu, S. Wang, Y. Ye, X. Song and Z. Liang, *Microporous and Mesoporous Materials*, 2022, **336**, 111871.
22. B. Tai, B. Li, L. He, Z. Ma, S. Lin, M. Zhang, J. Chen, F. Wu, L. Chen, X. Dai, F. Ma, Z. Chai and S. Wang, *Science China Chemistry*, 2024, **67**, 1569-1577.
23. W.-Z. She, Q.-L. Wen, H.-C. Zhang, J.-Z. Liu, R. S. Li, J. Ling and Q. Cao, *ACS Applied Nano Materials*, 2023, **6**, 18177-18187.
24. L. He, L. Chen, X. Dong, S. Zhang, M. Zhang, X. Dai, X. Liu, P. Lin, K. Li, C. Chen, T. Pan, F. Ma, J. Chen, M. Yuan, Y. Zhang, L. Chen, R. Zhou, Y. Han, Z. Chai and S. Wang, *Chem*, 2021, **7**, 699-714.
25. S. Fajal, D. Majumder, W. Mandal, S. Let, G. K. Dam, M. M. Shirolkar and S. K. Ghosh, *Journal of Materials Chemistry A*, 2023, **11**, 26580-26591.